JOURNAL OF COMPUTATIONAL PHYSICS 19, 211–228 (1975)

Local Mesh Refinement Using Rectangular Blended Finite Elements

JAMES C. CAVENDISH

Mathematics Department, Research Laboratories, General Motors Corporation, Warren, Michigan 48090

Received March 10, 1975

In a recent note [1], Birkhoff, Cavendish, and Gordon proposed a new and quite general class of piecewise polynomial *rectangular* finite elements which are easily constructed by local linear blending of simple univariate functions. Local mesh refinement is made easy for these new blended finite elements by removal of the usual requirement of vertex to vertex connection between adjacent elements so that two or more smaller elements can abut against the edge of a larger element. In addition, these elements can be modified to provide finite element approximations which exactly satisfy prescribed Dirichlet boundary conditions on the boundary of any bounded, (possibly) multiply connected rectangular polygon. The present paper explores these new techniques in detail and provides numerical examples which illustrate that high accuracy can be obtained and efficiency improved by using such locally refined, rectangular blended elements in finite element calculations.

1. INTRODUCTION

Nonsmooth elliptic boundary value problems occur frequently in practical engineering applications. For example, the exact solution may involve singularities, as is almost automatically the case for domains with corners, in material interface problems, or in problems involving source/sink driving functions. It is generally agreed that standard triangular elements (enriched when appropriate with singular functions) are more adaptable than rectangular elements for the approximation of such problems with the finite element method. This preference often stems from the relative ease with which *local mesh refinement* can be effected by the use of triangular elements.

Recently, a technique based on linear blending function theory [2, 9] was proposed for the derivation of new, rectangular, piecewise polynomial finite element types [1] and for which local mesh refinement is easily effected.[1] These new elements

[1] For earlier treatments of blended elements see [3, 4, 10, 11, 15].

differ from standard piecewise polynomial finite elements in that vertex to vertex connection for adjacent elements is *not* required during element assembly, and thus two or more smaller elements are allowed to abut against the edge of a larger element.

Let Ω be any bounded rectangular polygon and let π be a decomposition of Ω into an *arbitrary* disjoint union of rectangles. In Figs. 1–4 we give examples which illustrate the kinds of locally refined arrays of rectangular elements which we have in mind. Note that some of the *mesh lines* of π terminate in the interior of Ω.

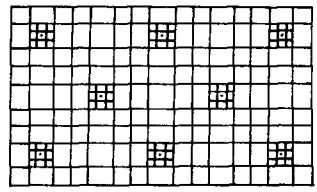

FIG. 1. Local mesh refinement about eight points.

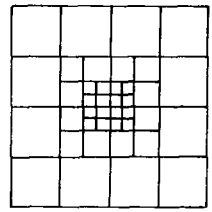

FIG. 2. A second scheme for local mesh refinement about a point.

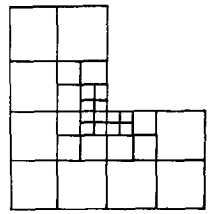

FIG. 3. Local mesh refinement at reentrant corner of L-shaped region.

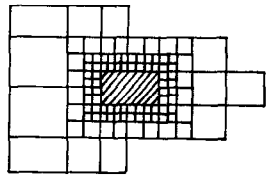

FIG. 4. Local mesh refinement for a doubly connected rectangular polygon.

In Section 2, we show how these new piecewise polynomial blended elements are constructed. In addition, we indicate how these elements can be modified near the boundary of Ω to provide finite element approximations which *exactly* satisfy prescribed Dirichlet boundary conditions.

The results of numerical calculations are presented in Section 3 for three model problems: (1) the determination of displacement near the point of application of a point loaded membrane, (2) the determination of deformation of a cracked beam under torsion, and (3) a point source problem with nonhomogeneous Dirichlet boundary conditions. The main conclusion reached from these calculations is that the use of locally refined, linearly blended finite elements is an efficient technique for the approximation of nonsmooth boundary value problems.

2. The Linearly Blended Finite Element Subspace, $S^h(\pi)$

Let Ω be a bounded, possibly multiply connected rectangular polygon which has been decomposed *arbitrarily* into a disjoint union π of *rectangular* cells, $\Omega_1, \Omega_2, \ldots, \Omega_N$ by *mesh lines* drawn parallel to the x and y coordinate axes; and such that a total of M *mesh nodes* (vertices) $P_1, P_2, \ldots, P_M$ results. In Fig. 3, for example, $N = 30$ and $M = 47$. Let $\partial\Omega_1, \partial\Omega_2, \ldots, \partial\Omega_N$ represent the boundaries of the cells, and let h denote the maximum length of all cell sides.

The approximation scheme to be considered assigns to each set of *nodal values* $v_j \equiv v(P_j)$ a *continuous, piecewise bilinear interpolant* v^h defined on Ω as follows.

(i) Construct continuous, univariate, piecewise linear interpolants to the nodal values v_j along *each* vertical and horizontal mesh line using as *joints* the adjacent mesh nodes in π.

(ii) Within each mesh cell Ω_p, define v^h to be the *linearly blended interpolant*

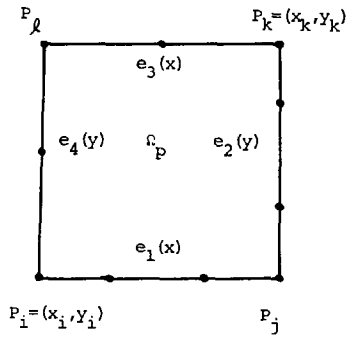

FIG. 5. The element Ω_p.

[2, 9] to the resulting piecewise linear boundary functions defined on the four edges of Ω_p by (i).

Let us be more specific. If Ω_p is an arbitrary cell in π, then the mesh nodes P_i *associated* with Ω_p are those nodes which lie on $\partial\Omega_p$ (see Fig. 5).

Now let $e_1(x)$, $e_2(y)$, $e_3(x)$, and $e_4(y)$ be univariate functions defined on the respective edges $\overline{P_iP_j}$, $\overline{P_jP_k}$, $\overline{P_kP_l}$, and $\overline{P_lP_i}$ of Ω_p (cf. Fig. 5). The e functions (called *edge functions* in the sequel) are assumed only to be *compatible* (i.e., $e_1(x_i) = e_4(y_i)$, etc.). Linear blending [2, 9] of these edge functions defines the interpolant

$$\begin{aligned} v(x, y) \equiv\ & e_4(y)\left[\frac{x_k - x}{x_k - x_i}\right] + e_2(y)\left[\frac{x - x_i}{x_k - x_i}\right] + e_1(x)\left[\frac{y_k - y}{y_k - y_i}\right] \\ & + e_3(x)\left[\frac{y - y_i}{y_k - y_i}\right] - e_1(x_i)\left[\frac{x_k - x}{x_k - x_i}\right]\left[\frac{y_k - y}{y_k - y_i}\right] \\ & - e_1(x_k)\left[\frac{x - x_i}{x_k - x_i}\right]\left[\frac{y_k - y}{y_k - y_i}\right] - e_3(x_k)\left[\frac{x - x_i}{x_k - x_i}\right]\left[\frac{y - y_i}{y_k - y_i}\right] \\ & - e_3(x_i)\left[\frac{x_k - x}{x_k - x_i}\right]\left[\frac{y - y_i}{y_k - y_i}\right]. \end{aligned} \tag{1}$$

Note that $v(x, y)$ interpolates exactly the edge functions on $\partial\Omega_p$.

If the edge functions in (1) are all defined to be compatible piecewise linear functions with joints located at the mesh nodes associated with Ω_p, then it follows from (1) that the resulting function v^h is *continuous, piecewise bilinear* on Ω_p with respect to the *tensor product* partition shown in Fig. 6.

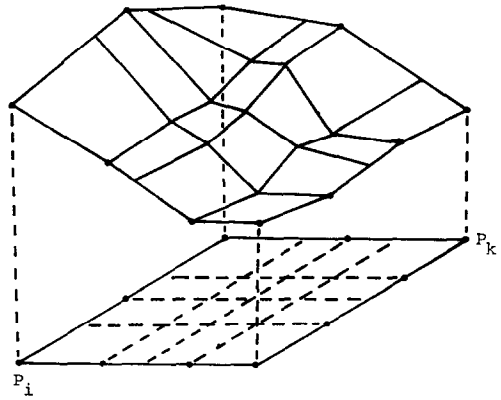

FIG. 6. v^h defined on Ω_p.

A cell is called *simple* if the only nodes associated with it are its four corner nodes. It follows from (1) that v^h is bilinear on a simple cell Ω_p (i.e., $v^h = a_0 + a_1x + a_2y + a_3xy$), hence (Ω_p, v^h) is the familiar bilinear finite element with four degrees of freedom. If Ω_p is a nonsimple cell, then v^h is piecewise bilinear on Ω_p (cf. Fig. 6) and (Ω_p, v^h) is in fact a *macroelement* [12, p. 84] with interior nodal values constrained a priori by construction.

If v^h is defined on Ω via its local definition on each Ω_p, then v^h is uniquely determined by its nodal values $v^h(P_j), j = 1, 2,..., M$. Note also that v^h is continuous on all of Ω and hence has finite strain energy (i.e., the Dirichlet integral $\iint_\Omega (\nabla v^h \cdot \nabla v^h)\, dx\, dy$ is bounded). Therefore, if $S^h(\pi)$ is defined to be the collection of all v^h as $(v^h(P_1), v^h(P_2),..., v^h(P_M))$ ranges over R^M, then $S^h(\pi)$ is an M-dimensional admissible trial solution space for finite element approximations to second-order elliptic boundary value problems. A slight modification of the convergence proof in [1] shows that if $u(x, y)$ is a sufficiently smooth function defined on Ω, then

$$\| u - \tilde{u}^h \| = O(h),$$

where $\| \cdot \|$ is the norm $\| v \|^2 \equiv \iint_\Omega \{v^2 + v_x^2 + v_y^2\}\, dx\, dy$ and $\tilde{u}^h \in S^h(\pi)$ is characterized by $\tilde{u}^h(P_i) = u(P_i), i = 1, 2,..., M$.

If we define $S_0^h(\pi)$ to be the subspace of functions in $S^h(\pi)$ which vanish on $\partial\Omega$, then it follows that $v^h \in S_0^h(\pi)$ if and only if $v^h(P_i) = 0$ for all $P_i \in \partial\Omega$.

Finally, let $g(x, y)$ be a given function defined on $\partial\Omega$ (a Dirichlet boundary condition, for example) and let Ω_p be any cell in π. For those edges of Ω_p which lie *in* $\partial\Omega$, let the corresponding e functions in (1) be given by the appropriate values of $g(x, y)$, while for edges of $\partial\Omega$ which do not lie in $\partial\Omega$, let the corresponding compatible e functions be piecewise linears defined by the interpolation conditions

$$\begin{aligned} e(P_i) &= g(P_i) \qquad \text{if} \quad P_i \in \partial\Omega, \\ e(P_i) &= 0 \qquad\quad \text{if} \quad P_i \notin \partial\Omega. \end{aligned}$$

Let the resulting linear blended interpolant in (1) be denoted $G^h(x, y)$. Note that if G^h is extended to all of Ω by its local definition on Ω_p, then $G^h \equiv g$ on $\partial\Omega$ and $G^h \equiv 0$ on all Ω_p such that $\Omega_p \cap \partial\Omega$ is empty. The locally refined trial solution space defined by $G^h + S_0^h(\pi)$ can now be used to provide finite element approximations $u^h \equiv G^h + v^h$ which *exactly* satisfy the boundary condition $u = g$ on $\partial\Omega$.[2]

Before considering numerical results, we describe a computationally convenient basis for the space $S^h(\pi)$. Let $\phi_j(x, y)$ be the trial function in $S^h(\pi)$ which equals 1 at the jth node and zero at all other nodes in π. Then these linearly blended

[2] This exact boundary technique was first proposed for finite element analysis by Marshall and Mitchell [11] for bilinear tensor product elements.

functions ϕ_j form a *patch basis* for the trial space $S^h(\pi)$; that is, ϕ_j vanishes on all elements not containing the jth node. Using this basis for numerical calculations, we focus now on the implementation of locally refined, linearly blended elements for the finite element approximation of three boundary value problems.

3. Numerical Results

For our first problem we consider the determination of displacement near the point of application of a point loaded rectangular membrane.

The Point Loaded Membrane

Consider the simple displacement problem for a clamped square membrane subject to a point load applied at its center. The displacement u is characterized by the boundary value problem

$$-\nabla^2 u = f(x, y) = \delta(x - \tfrac{1}{2}, y - \tfrac{1}{2}) \quad \text{for} \quad (x, y) \in \Omega = (0, 1) \times (0, 1), \tag{2}$$

$$u = 0 \quad \text{for} \quad (x, y) \in \partial\Omega, \tag{3}$$

and u behaves radially at $(\frac{1}{2}, \frac{1}{2})$ like $\ln r$. Let $S_0^h(\pi)$ be the space of linearly blended trial functions which vanish on $\partial\Omega$. The finite element approximation $u^h \in S_0^h(\pi)$ is defined to be that function in $S_0^h(\pi)$ that satisfies

$$\iint_\Omega \{u_x^h v_x + u_y^h v_y\} = \iint_\Omega \{fv\} \equiv v(\tfrac{1}{2}, \tfrac{1}{2}) \qquad \text{for all} \quad v \in S_0^h(\pi).$$

We begin by defining a sequence of locally refined rectangular partitions π_n, $n = 1, 2, \ldots$ of Ω. In Figs. 7–9 we show π_1, π_2, and π_3, and from these constructions it should be clear how π_n is derived as a local refinement of π_{n-1}. Note that each π_n is a nested union of *square* elements with the maximum side length of any element being $\bar{\pi}_n = \frac{1}{4}(\frac{1}{2})^{n-1}$. Also, $\dim S_0^h(\pi_n) = 16n - 7$.

In Fig. 10 we plot the plane sectional values of displacement u and approximate

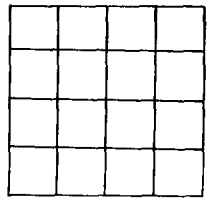

Fig. 7. Partition π_1 for membrane problem.

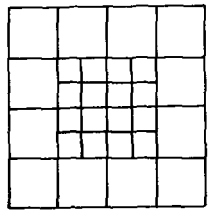

FIG. 8. Partition π_2 for membrane problem.

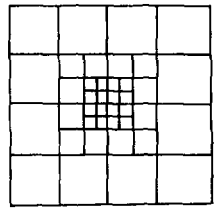

FIG. 9. Partition π_3 for membrane problem.

displacement u^h determined along the 45° line $y = x$ for the partitions π_1, π_3, and π_5. The values of the exact solution $u(x, y)$ were calculated from the representation given in [5, p. 386]. As anticipated, local mesh refinement results in improved accuracy without the expense of a large increase in the number of unknowns in the finite element problem.

Torsion Problem

For our second problem (Fix, Gulati, and Wakoff [7]) we consider the boundary value problem

$$-\nabla^2 u = 1 \qquad \text{on } \Omega, \tag{4}$$

$$\begin{aligned} u &= 0 \qquad \text{on } PP_1, P_2P_3, \\ \partial u/\partial \eta &= 0 \qquad \text{on } P_1P_2, Q_2P_3, PQ_2, \end{aligned} \tag{5}$$

where Ω is the rectangle $[0, 1] \times [0, \frac{1}{2}]$ (see Fig. 11). This boundary value problem arises in the study of the rigidity and deformation of a cracked square elastic beam under torsion (see [7] for details).

The solution u to (4) and (5) has a singularity only at the point $P = (\frac{1}{2}, \frac{1}{2})$, which behaves radially at P like $r^{1/2} \sin \theta/2$. The so-called *stress intensity factor*, σ_0, associated with (4) and (5) is defined by

$$\sigma_0 = \lim_{r \to 0} r^{-1/2}[u(r, \pi)]. \tag{6}$$

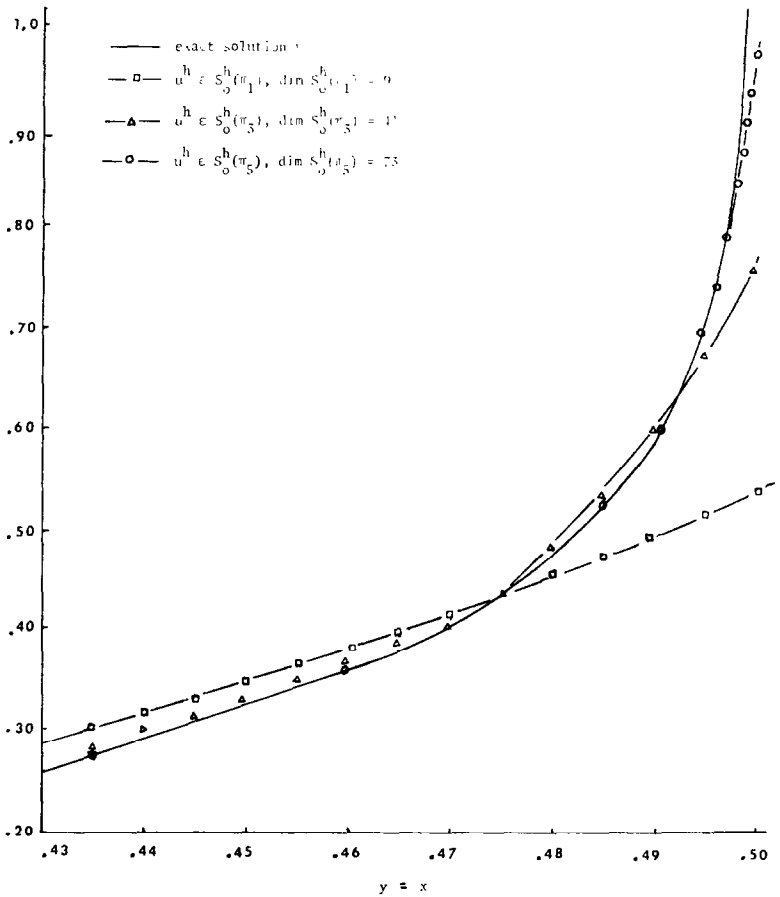

FIG. 10. Plots of exact solution u to source problem (2), (3), and finite element approximations u^h in $S_0^h(\pi_n)$ for $n = 1, 3$, and 5.

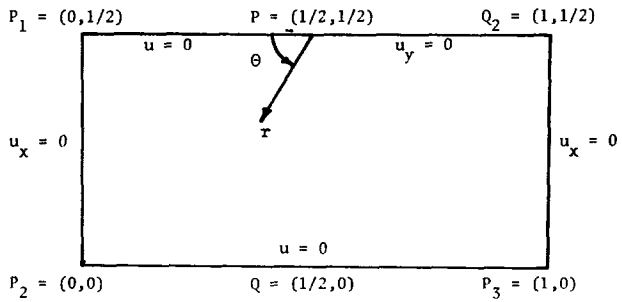

FIG. 11. The domain Ω.

Our aim is to provide accurate approximations to σ_0 using finite element approximations u^h generated in the linearly blended finite element space $S_0^h(\pi)$ (in this case the members of $S_0^h(\pi)$ need only be forced to satisfy the essential Dirichlet boundary conditions given in (5)). To this end we define a sequence $\{\pi_n\}$ of locally refined rectangular decompositions of Ω. In Figs. 12–14 we show

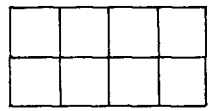

FIG. 12. The partition π_1 for the crack problem.

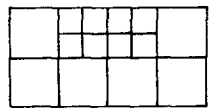

FIG. 13. The partition π_2 for the crack problem.

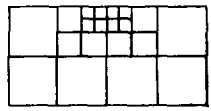

FIG. 14. The partition π_3 for the crack problem.

π_1, π_2, and π_3 from these figures it should be clear how π_n is constructed as a local refinement of π_{n-1}. Note again that for any n, π_n is composed solely of square elements with maximum side length $\bar{\pi}_n = \frac{1}{4}$ and minimum side length $\underline{\pi}_n = \frac{1}{4}(\frac{1}{2})^{n-1} = (\frac{1}{2})^{n+1}$, $n = 1, 2,\ldots$. By counting the number of unconstrained node points in π_n, it is easy to verify that

$$\begin{aligned} \dim(S_0^h(\pi_n)) &= \dim(S_0^h(\pi_{n-1})) + 8 \\ &= 8n - 1 \qquad \text{for} \quad n = 1, 2,\ldots. \end{aligned} \tag{7}$$

By virtue of (7), the symmetric, banded finite element stiffness matrix $K_{LB}(\pi_n)$, which arises from calculations in $S_0^h(\pi_n)$, is an $(8n - 1) \times (8n - 1)$ matrix for $n = 1, 2,\ldots$. Let $M_{LB}(\pi_n)$ represent the *bandwidth* of $K_{LB}(\pi_n)$. That is to say, $M_{LB}(\pi_n)$ is the number of strictly upper diagonals in $K_{LB}(\pi_n)$. Now suppose that the unknowns in $S_0^h(\pi_n)$ are ordered according to the *nested* scheme shown for π_3 in Fig. 15. From Fig. 15 it should be clear how this nested ordering would be defined for π_n, $n = 1, 2,\ldots$. From Fig. 15 it can be easily verified that

$$M_{LB}(\pi_n) = 10 \qquad \textit{for all } n = 1, 2,\ldots. \tag{8}$$

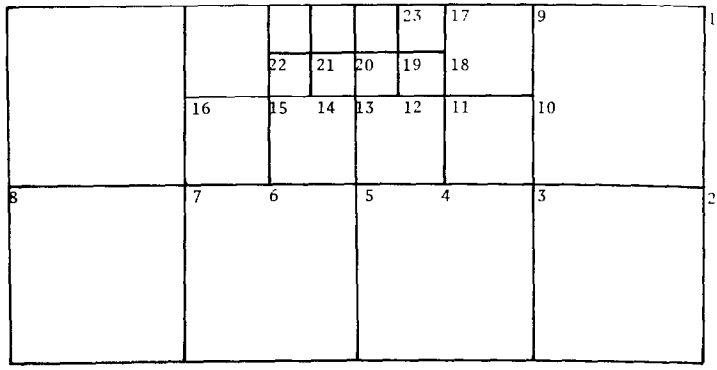

FIG. 15. A nested ordering of unknowns in π_3.

Finally, if u^h is the linearly blended finite element approximation to u in $S_0^h(\pi_n)$, then we define $\sigma_n(r^*) \cong \sigma_0$ by (cf. (7))

$$\sigma_n(r^*) \equiv u^h(r^*, \pi)/(r^*)^{1/2}, \tag{9}$$

where r^* is a small positive number. The exact value of σ_0 determined in [7] is given by $\sigma_0 = 0.1917$. In Table I we show the results of determining $\sigma_n(r^*)$ in (9) using $u^h \in S_0^h(\pi_n)$ for $n = 12$, 15, 18, and 21. For this table the values $r^* = (\frac{1}{2})^{10}$, $(\frac{1}{2})^{11}$, $(\frac{1}{2})^{12}$ and $(\frac{1}{2})^{13}$ were used.

Table II gives the values for the approximate stress function u^h at the points with coordinates $R_1 = (12/24, 11/24)$, $R_2 = (1/24, 1/4)$ and $R_3 = (23/24, 1/4)$ for

TABLE I

An Approximation to Stress Intensity Factor σ_0 for Crack Problem Using Linearly Blended Finite Elements in $S_0^h(\pi_n)$ to Calculate σ_n ($\sigma_0 = 0.1917$)

n	Dim $S_0^h(\pi_n)$ $= 8n - 1$	$M_{LB}(\pi_n)$	$\sigma_n(r^*)$ [a]	$\sigma_n(r^*)$ [b]	$\sigma_n(r^*)$ [c]	$\sigma_n(r^*)$ [d]
12	95	10	0.1895	0.1875	0.1837	0.1788
15	119	10	0.1913	0.1912	0.1908	0.1898
18	143	10	0.1915	0.1916	0.1917	0.1917
21	167	10	0.1917	0.1917	0.1917	0.1917

[a] $r^* = (\frac{1}{2})^{10}$.
[b] $r^* = (\frac{1}{2})^{11}$.
[c] $r^* = (\frac{1}{2})^{12}$.
[d] $r^* = (\frac{1}{2})^{13}$.

TABLE II

Linearly Blended Finite Element Approximations in the Space $S_0^h(\pi_n)$ to the Stress Function Calculated at the Points R_1, R_2, and R_3

n	Dimension of $S_0^h(\pi_n)$	$u^h(R_1)$ [a]	$u^h(R_2)$ [b]	$u^h(R_3)$ [c]
1	7	0.007423	0.03189	0.06685
3	23	0.02070	0.03375	0.07032
6	47	0.02650	0.03387	0.07105
12	95	0.02694	0.03388	0.07105

[a] $R_1 = (12/24, 11/24)$, $u(R_1) = 0.027425$.
[c] $R_2 = (1/24, 1/4)$, $u(R_2) = 0.032877$.
[c] $R_3 = (23/24, 1/4)$, $u(R_3) = 0.070844$.

the partitions π_1, π_3, π_6, and π_{12}. The exact values of u at R_1, R_2, and R_3 were determined in [7] to be, respectively, 0.027425, 0.032877, and 0.070844.

In order to provide comparison of locally refined, linearly blended finite elements with the technique of adjoining appropriate singular basis functions to standard piecewise polynomial finite element spaces, we consider the results presented in [7] for approximating (4) and (5). In [7] a uniform product partition of subsquares with side length h is first used to decompose the region Ω in Fig. 11. Next, piecewise polynomial, finite element spaces associated with the product partition of Ω are defined as follows.

(i) S_h^L denotes the space of continuous *bilinear polynomials* $a + bx + cy + dxy$ in each subsquare of Ω.

(ii) S_h^H denotes the space of C^1 functions which are *bicubic Hermite* polynomials in each subsquare of Ω.

(iii) S_h^{SL} is the space of piecewise bicubic polynomials of class C^2 everywhere except across the line PQ in Fig. 11 where they are only continuous.

To the spaces S_h^L, S_h^H, and S_h^{SL} are added singular functions (see [7, pp. 211–216] for details). Four singular basis functions are added to S_h^H and S_h^{SL}, while two singular basis functions are added to S_h^L. Finally, the spaces enriched with singular functions are denoted by SS_h^L, SS_h^H, and SS_h^{SL}.

In Table I′ we reproduce the results given in [7] for the approximate stress intensity factor σ_0^h defined using finite element approximations in SS_h^L, SS_h^H, and SS_h^{SL}. Table II′ gives the values of the finite element approximations in SS_h^L, SS_h^H, and SS_h^{SL} at the points R_1, R_2, R_3 defined in Table II.

TABLE I′

Approximate Stress Intensity Factor $\sigma_0{}^h$ Using Singular Finite Element Approximations

Space	Dimension (h)	$\sigma_0{}^h$ (0.1917)
SS_h^{SL}	40(1/6)	0.1925
	59(1/8)	0.1920
	109(1/12)	0.1918
$SS_h{}^H$	36(1/4)	0.1902
	132(1/8)	0.1915
	204(1/10)	0.1916
$SS_h{}^L$	33(1/8)	0.1830
	129(1/16)	0.1867
	201(1/20)	0.1877

TABLE II′

Singular Finite Element Approximation to the Solution of Eqs. (4) and (5)

Space	Dimension (h)	R_1 0.027425	R_2 0.032877	R_3 0.070844
SS_h^{SL}	40(1/6)	0.027438	0.032887	0.070835
	59(1/8)	0.027429	0.032881	0.070847
	109(1/12)	0.027426	0.032877	0.070844
$SS_h{}^H$	36(1/4)	0.027402	0.032859	0.070895
	132(1/8)	0.027423	0.032876	0.070848
	204(1/10)	0.027424	0.032877	0.070844
$SS_h{}^L$	33(1/8)	0.026459	0.033025	0.070385
	129(1/16)	0.027153	0.032917	0.070721
	201(1/30)	0.027289	0.032903	0.070780

Comparison of Table I with Table I′ and Table II with Table II′ shows that finite element calculations using locally refined, linearly blended finite elements compare favorably (if system dimensionality is the basis for comparison) with like calculations performed in the piecewise polynomial spaces which have been augmented by singular functions. We remark that convergence is numerically demonstrated

in Table II′ as $h \to 0$ for finite element approximations in SS_h^L, SS_h^H, and SS_h^{SL}. That numerical convergence is *not* demonstrated in Table II for approximations in $S_0^h(\pi_n)$ is attributable to the fact that an increase in n in Table II implies a *local* refinement of π_n ($h = \bar{\pi} = \frac{1}{4}$ remains constant for all n) about the point P in Fig. 11, while a decrease in h in Table II′ implies a *global* refinement in the product partition of the entire region Ω. Convergence in $S_0^h(\pi_n)$ is, of course, achieved as $h \to 0$.

Let Π_n be the decomposition of Ω into rectangles defined by extending to $\partial\Omega$ all those mesh lines in π_n which have terminal points interior to Ω. Π_n is said to be a *semilocal product* mesh refinement of Ω. Since all cells in Π_n are simple cells, the space $S_0^h(\Pi_n)$ of linearly blended finite elements defined in Section 2 is, in fact, the familiar *tensor product* space of rectangular bilinear finite elements associated with Π_n with four degrees of freedom per element. If the nodal unknowns in $S_0^h(\Pi_n)$ are ordered from left to right, a line at a time as usual, then it is easily verified that

$$\dim S_0^h(\Pi_n) = 2n^2 + 4n + 1, \tag{10}$$

$$M_{LB}(\Pi_n) = 2(n + 2), \tag{11}$$

where $M_{LB}(\Pi_n)$ is the bandwidth of the stiffness matrix defined by finite element approximations to (4) and (5) in $S_0^h(\Pi_n)$.

In Table III we give the numerical results of approximating the stress intensity factor σ_0 by $\sigma_n(r^*)$ in (9) using u^h in $S_0^h(\Pi_n)$ for $n = 12$, 15, and 18. The conclusions to be drawn from a comparison of Tables I and III are obvious: Accurate approximations to σ_0 using finite element approximations in the locally refined space

TABLE III

Approximation to Stress Intensity Factor σ_0 for Crack Problem Using Bilinear Tensor Product Finite Elements in $S_0^h(\Pi_n)$ to Calculate σ_n ($\sigma_0 = 0.1917$)

n	Dim $S_0^h(\Pi_n)$ $= 2n^2 + 4n + 1$	$M_{LB}(\Pi_n)$ $= 2n + 4$	$\sigma_n(r^*)$ [a]	$\sigma_n(r^*)$ [b]	$\sigma_n(r^*)$ [c]	$\sigma_n(r^*)$ [d]
12	337	28	0.1898	0.1878	0.1834	0.1788
15	511	34	0.1916	0.1915	0.1910	0.1898
18	721	40	0.1917	0.1917	0.1917	0.1917

[a] $r^* = (\frac{1}{2})^{10}$.
[b] $r^* = (\frac{1}{2})^{11}$.
[c] $r^* = (\frac{1}{2})^{12}$.
[d] $r^* = (\frac{1}{2})^{13}$.

$S_0^h(\pi_n)$ can be obtained with far fewer unknowns than similar approximations in the semilocally refined bilinear space $S_0^h(\Pi_n)$.

A Source Problem: Exact Representation of Boundary Conditions

Our final example (Marshall and Mitchell [11]) involves nonhomogeneous Dirichlet boundary conditions, $u = g$ on $\partial\Omega$, and is included to illustrate the results of performing finite element calculations in the space $G^h + S_0^h(\pi)$, where G^h is the linearly blended interpolant of g defined in Section 2 such that $G^h \equiv g$ on $\partial\Omega$.

For $\epsilon > 0$, consider the problem

$$\nabla^2 u = 0 \qquad \text{on} \quad \Omega = (0, 1) \times (0, 1) \tag{12}$$

with boundary condition

$$u = g \equiv \ln r \qquad \text{on} \quad \partial\Omega, \tag{13}$$

where $r^2 \equiv (x + \epsilon)^2 + (y + \epsilon)^2$. The exact solution u to this problem is given by

$$u = \ln r \qquad \text{for} \quad (x, y) \text{ in } \bar{\Omega}.$$

Note that u possesses high local gradient near the origin with $\| \nabla u \| = 1/r$ in Ω and $\| \nabla u \| \doteq 0.707/\epsilon$ for $(x, y) = (0, 0)$.

Let $\{\pi_n\}$ be the sequence of locally refinement rectangular partitions of Ω defined in Figs. 16–18 for $n = 1$, 2, and 3.

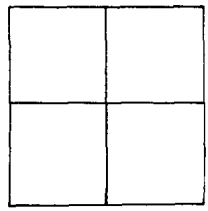

FIG. 16. The partition π_1.

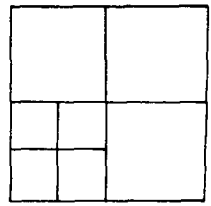

FIG. 17. The partition π_2.

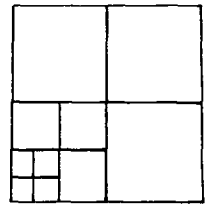

FIG. 18. The partition π_3.

Let $\{\Pi_n\}$ be the sequence of tensor product, semilocally refined partitions of Ω, where π_n is defined by *extending* the mesh lines of π_n through to $\partial\Omega$. As before, $S_0^h(\pi_n)$ is the locally refined space of linearly blended elements, and $S_0^h(\Pi_n)$ is the standard semilocally refined tensor product space of bilinear elements.

Next, let $\tilde{g}(\pi_n)$ and $\tilde{g}(\Pi_n)$ represent *discrete piecewise linear interpolants* to the boundary function g in (13) defined with respect to the *boundary* mesh nodes in π_n and Π_n, respectively, and let $G^h(\pi_n)$, $\tilde{G}^h(\pi_n)$ and $\tilde{G}^h(\Pi_n)$ be, respectively, the linearly blended interpolants of g, $\tilde{g}(\pi_n)$, and $\tilde{g}(\Pi_n)$ as defined in Section 2. We now consider finite element approximations to (12) and (13) generated in the three functions spaces $G^h(\pi_n) + S_0^h(\pi_n)$, $\tilde{G}^h(\pi_n) + S_0^h(\pi_n)$, and $\tilde{G}^h(\Pi_n) + S_0^h(\Pi_n)$. Table IV we list the characteristics of each of the approximation spaces.

TABLE IV

Characteristics of Approximation Spaces

Space	Dim $S_0^h(\cdot)$	Bandwidth of stiffness matrix	Value on $\partial\Omega$	Type of refinement
$G^h(\pi_n) + S_0^h(\pi_n)$	$3n - 2$	3^a	g	Local
$\tilde{G}^h(\pi_n) + S_0^h(\pi_n)$	$2n - 2$	3^a	$\tilde{g}(\pi_n)$	Local
$\tilde{G}^h(\Pi_n) + S_0^h(\Pi_n)$	n^2	n^b	$\tilde{g}(\Pi_n)$	Semilocal

[a] Based on nested ordering of unknowns similar to Fig. 15.
[b] Based on usual ordering of tensor product unknowns.

The finite element approximation $u^h \equiv G^h(\pi_n) + v^h$ in $G^h(\pi_n) + S_0^h(\pi_n)$ to u is characterized by

$$(\nabla(G^h(\pi_n) + v^h), \nabla v) = 0 \qquad \text{for all } v \text{ in } S_0^h(\pi_n),$$

where $(,)$ is the usual L_2-inner product on Ω. Similar characterizations hold for u^h in $\tilde{G}^h(\pi_n) + S_0^h(\pi_n)$ and $\tilde{G}^h(\Pi_n) + S_0^h(\Pi_n)$. We remark that $u_h \in \tilde{G}^h(\Pi_n) +$

$S_0^h(\Pi_n)$ is a standard tensor product finite element approximation to (12) and (13) in which the boundary condition has been approximated by piecewise linear interpolation.

Let $\epsilon = 10^{-5}$ in (13) so that $\| u \| \doteq 10^5$ at (0, 0). In Tables V, VI, and VII we give the numerical results of approximating u by its finite element approximation

TABLE V

Finite Element Approximation to Eqs. (12) and (13) in $G^h(\pi_n) + S_0^h(\pi_n)$

n	Dim $S_0^h(\pi_n)$	Bandwidth of stiffness matrix	$\| u - u^h \|_\infty$	(Relative error)
8	22	3	2.41	(34.0%)
10	28	3	1.44	(17.7%)
12	34	3	0.67	(7.3%)

Note. $u^h \in G^h(\pi_n) + S_0^h(\pi_n)$.

TABLE VI

Finite Element Approximation to Eqs. (12) and (13) in $\tilde{G}^h(\pi_n) + S_0^h(\pi_n)$

n	Dim $S_0^h(\pi_n)$	Bandwidth of stiffness matrix	$\| u - u^h \|_\infty$	(Relative error)
8	22	3	4.29	(67.1%)
12	34	3	1.92	(21.8%)
14	40	3	0.96	(9.92%)

Note. $u^h \in \tilde{G}^h(\pi_n) + S_0^h(\pi_n)$.

TABLE VII

Finite Element Approximation to Eqs. (12) and (13) in $\tilde{G}^h(\Pi_n) + S_0^h(\Pi_n)$

n	Dim $S_0^h(\Pi_n)$	Bandwidth of stiffness matrix	$\| u - u^h \|_\infty$	(Relative error)
8	64	8	2.91	(40.1%)
10	100	10	1.83	(21.8%)
12	144	12	0.91	(9.73%)

Note. $u^h \in \tilde{G}^h(\Pi_n) + S_0^h(\Pi_n)$.

u^h in $G^h(\pi_n) + S_0{}^h(\pi_n)$, $\tilde{G}^h(\pi_n) + S_0{}^h(\pi_n)$, and $\tilde{G}^h(\Pi_n) + S_0{}^h(\Pi_n)$, respectively. In these tables $\| \cdot \|_\infty$ signifies the *maximum* norm. As expected, for a given dimensionality, approximations in $G^h(\pi_n) + S_0{}^h(\pi_n)$ are more accurate than similar approximations in $\tilde{G}^h(\pi_n) + S_0{}^h(\pi_n)$; and this improvement is most noticeable for coarse partitions. Comparing Tables V and VI with VII indicates, however, that local mesh refinement is the most important factor (as opposed to the exact representation of boundary conditions) in improving the efficiency of the finite element calculations.

4. Conclusions and Comments

We have described the construction and use of a finite dimensional, piecewise bilinear, space of linearly blended finite elements. When used as a trial solution space, this class of functions permits locally refined rectangular partitions of any bounded rectangular polygon Ω. Numerical calculations indicate that finite element approximations can be generated in these spaces which yield accurate approximations to boundary value problems possessing local regions of high gradients without the expense of an unreasonably large number of finite element nodal unknowns.

We wish to point out that although the region Ω has been assumed throughout to be a rectangular polygon, the linearly blended elements discussed in this paper can be abuted against any element that yields linear displacement along the adjoining adge (for example, linear triangles or curved isoparametric triangles with at least one linear side [16]). Such a merger would yield continuous approximations and would exploit the greater flexibility of triangular elements for approximating curved boundaries.

As pointed out in [1], *higher order* linearly blended elements can be constructed by considering higher order piecewise polynomial edge functions in (1) than the piecewise linears considered in Section 2 (for example, cubic spline or cubic Hermite polynomials). We presume that the conclusions we have reached in this paper would not be changed were such extensions to be implemented.

Acknowledgment

The author thanks Professor Garrett Birkhoff and Dr. William Gordon for their helpful discussions and for their careful reading of the manuscript.

References

1. G. Birkhoff, J. C. Cavendish, and W. J. Gordon, *Proc. Nat. Acad. Sci.* **9** (1974), 3423–3425.
2. G. Birkhoff and W. J. Gordon, *J. Approximation Theory* **1** (1968), 199–208.

3. J. C. CAVENDISH, W. J. GORDON, AND C. A. HALL, Ritz-Galerkin Approximations in Blending Function Spaces, I. Approximation Theoretic Analysis, to appear in *Numer. Math.* (also available as General Motors Research Publication GMR-1572).
4. J. C. CAVENDISH, W. J. GORDON, AND C. A. HALL, Ritz-Galerkin Approximations in Blending Function Spaces, II. Computational Aspects, submitted to *Numer. Math.* (also available as General Motors Research Publication GMR-1572 Part II).
5. R. COURANT AND D. HILBERT, "Methods of Mathematical Physics," Vol. I, Interscience, New York, 1953.
6. S. C. EISENSTAT AND M. H. SCHULTZ, Computational Aspects of the Finite Element Method in "The Mathematical Foundations of the Finite Element Method with Applications to Partial Differential Equations," pp. 505–524, Academic Press, New York, 1972.
7. G. FIX, S. GULATI, AND G. I. WAKOFF, *J. Computational Phys.* **13** (1973), 209–228.
8. A. GEORGE, *SIAM J. Numer. Anal.* **10** (1973), 345–363.
9. W. J. GORDON, *SIAM J. Numer. Anal.* **8** (1971), 158–177.
10. W. J. GORDON AND C. A. HALL, *Numer. Math.* **21** (1973), 109–129.
11. J. A. MARSHALL AND A. R. MITCHELL, *J. Inst. Math. Appl.* **12** (1973), 355–362.
12. G. STRANG AND G. FIX, "Analysis of the Finite Element Method," Prentice–Hall, Englewood Cliffs, N.J., 1973.
13. B. K. SWARTZ AND R. S. VARGA, *J. Approximation Theory* **6** (1972), 6–49.
14. R. WAIT AND A. R. MITCHELL, *J. Computational Phys.* **8** (1971), 45–52.
15. D. WATKINS, Ph.D. Thesis, University of Calgary, 1974.
16. O. C. ZIENKIEWICZ, "The Finite Element Method in Engineering Science," McGraw–Hill, London, 1971.
17. M. ZLÁMAL, *SIAM J. Numer. Anal.* **10** (1973), 229–240.